Journal of The Electrochemical Society, **159** (5) C233-C243 (2012)
0013-4651/2012/159(5)/C233/11/$28.00 © The Electrochemical Society

Passivation of a CoCrMo PVD Alloy with Biomedical Composition under Simulated Physiological Conditions Studied by EQCM and XPS

C. Valero Vidal,[a,z] A. Igual Muñoz,[a] C.-O. A. Olsson,[b] and S. Mischler[b]

[a]*Departamento de Ingeniería Química y Nuclear, E.T.S.I. Industriales, Universidad Politécnica de Valencia, E-46071 Valencia, Spain*
[b]*Tribology and Interface Chemistry Group, Swiss Federal Institute of Technology Lausanne (EPFL), CH-1015 Lausanne, Switzerland*

Kinetics of passive film growth on a CoCrMo biomedical alloy have been studied using the Electrochemical Quartz Crystal Microbalance technique (EQCM) in phosphate buffer solution at room temperature and 37°C. CoCrMo layers were deposited on the quartz crystals by physical vapor deposition (PVD) reaching a dense and compact deposition film with fine-grain structure. EQCM measurements were performed under potentiodynamic and potentiostatic conditions (at applied passive and transpassive potentials). Furthermore, ex-situ X-ray Photoelectron Spectroscopy (XPS) analysis of the each tested sample was performed at the end of the electrochemical test. The use of EQCM allows distinguishing between electrochemical oxidation, passive and transpassive dissolution and passive film growth. In the passive domain the passive film thickness stabilizes within 200 to 400 s after an initial fast growth. The increase in current at the onset of the transpassive domain does not affect the passive dissolution rate. Only at higher potential dissolution rate increases due to the dissolution of Cr(VI), Co(III) and Mo(VI) species. The observed constant mass loss rate at transpassive potentials indicates that the passive film at these potentials is cracked or porous. Increasing temperature accelerates the mass loss through the oxide/electrolyte interface enhancing the passive and transpassive dissolution and increasing the thickness of the oxide film.
 [DOI: 10.1149/2.090205jes]

Manuscript submitted December 19, 2011; revised manuscript received February 21, 2012. Published March 5, 2012.

CoCrMo alloys are one of the most important metallic materials used in orthopedic implants.[1–3] Their use is based on their excellent mechanical properties (wear and hardness) and the high resistance to corrosion in physiological media which is related to the spontaneous formation of an oxide film that protects the metal from the surrounding environment. This layer has a high Cr content (mainly Cr_2O_3 and smaller amount of $Cr(OH)_3$) with a minor contribution of Co and Mo oxides.[4–7] One of the most important issues in the use of this metallic biomaterial is passive dissolution which has been considered one problem for the long term durability of the implants and for the adverse effects that can cause metal ion release (physiological effects, toxicity, carcinogenicity and metal allergy).[8–12] The properties of the oxide film may change depending on the physico-chemical conditions (i.e. temperature, potential, etc.) and the adsorption of organic species present in body fluids such as proteins.[13–15] Furthermore, there is an increasing interest in the study of interfacial behavior of proteins in the human body as a result of problems associated with bacterial growth[16,17] and metal dissolution.[18,19]

Considerable insight into the corrosion behavior of CoCrMo biomedical alloys has been obtained using conventional electrochemical techniques such as potentidynamic curves, cyclic voltammetry measurements, potentiostatic tests and Electrochemical Impedance Spectroscopy (EIS).[5,6,20–24] The Electrochemical Quartz Crystal Microbalance (ECQM) is known to be a powerful technique for studying the electrochemical process such as film modifications, mass transport phenomena and adsorption kinetics taking place at the interface of thin films.[25] This technique is based on the piezoelectric effect: the application of an applied electrical potential across the crystal induces a corresponding mechanical shear stress proportional to the applied potential.[26] Therefore, variations of the total mass occurring at the material surface can be measured quantitatively by a shift in the resonance frequency of the EQCM. The device is capable of measuring mass changes in the nanogram range.[27]

The total frequency change (Δf) obtained in an experimental EQCM measurement is due to the contribution of the mass loading (Δf_m) and the viscous loading (Δf_v) according to equation 1[28]:

$$\Delta f = \Delta f_m + \Delta f_v \qquad [1]$$

In the case of ideally smooth surfaces, rigidly attached films and Newtonians fluids, mass loading influences only the resonance frequency, whereas viscous loading affects both the frequency and the quartz crystal resistance near the resonance frequency.[28]

The mass loading is only related to changes in the total mass of the quartz due to mass added or removed from the surface. A relationship between the changes in the quartz electrode mass (Δm) and the frequency shift (Δf_m) due to mass loading was developed by Sauerbrey[27]:

$$\Delta f_m = -\frac{2 f_0^2}{N\sqrt{\rho_q \mu_q}} \cdot \Delta m = -C_f \cdot \Delta m \qquad [2]$$

where f_0 is the resonance frequency of the unloaded crystal (in MHz), ρ_q is the quartz density (in g cm^{-3}), μ_q is the elastic shear modulus of the quartz (in N cm^{-2}) and N is the harmonic resonance number ($N = 1$). C_f is the quartz sensitivity factor (in Hz cm^2 g^{-1}). According to Sauerbrey's theory, the mass sensitivity is only dependent the quartz properties, not the added material. Furthermore, the negative sign of the equation 2 shows an inverse relation between the frequency shift and the mass change on the electrode surface. Thus, a reduction in the resonant frequency is related to mass accumulating on the crystal.

Galliano et al.[28] demonstrated that the viscous loading Δf_v can be accurately corrected in real time by recording the crystal resistance ΔR_{crys} since a direct relation between the Δf_v and ΔR_{crys} exists according to Equation 3:

$$\Delta f_v = K \cdot \Delta R_{crys} \qquad [3]$$

Here K is a proportionality constant that need to be calibrated for a given system and temperature.

The EQCM technique has been employed in the study of passive films and electrochemical mechanisms (oxidation and dissolution) of a large number of metals and alloys.[29–37] For this reason, this technique has been used to investigate the corrosion of biomedical relevant metallic materials. EQCM corrosion studies have been carried out on titanium,[38–40] stainless steel[34,35] and chromium.[41,42] Frateur et al.[41] studied the adsorption of Bovine Serum Albumin (BSA) on passivated chromium and they observed very fast adsorption kinetics of the BSA on the metallic surface. Ithurbide et al.[42] studied the influence of potential and pH on the adsorption process of albumin on

[z] E-mail: carvavi@etsii.upv.es

passivated chromium surfaces. The adsorption kinetics were observed to be slightly dependent on the pH in the passive domain. No literature has been found related to the use of EQCM on the corrosion behavior of CoCrMo alloys. Further, it is interesting to note that all of the above mentioned authors carried out the EQCM tests at room temperature and not at body temperature (37°C). Knowing the large effect temperature has on electrochemical and absorption processes,[3] the possibility to extrapolate the published results to the in-vivo conditions appears problematic.

The main advantage of the EQCM is the possibility to measure the mass changes on an electrode surface in real time with high resolution and sensitivity. However, the EQCM is not able to differentiate between the dissolution of the alloy and passive film growth since only the overall mass change occurring on the electrode surface is measured. To get information on the chemical composition and thickness of the passive films, methods of surface analysis such as X-Photoelectron Spectroscopy (XPS) are needed. Thus XPS and EQCM were advantageously combined in the investigation of passivity, in particular for determining the film growth kinetics.[35–37]

The goal of this work is to study the anodic behavior of a CoCrMo biomedical alloy in simulated body fluids at room temperature and at 37°C. For this, the mass changes during potential sweeps from a low to a higher passive potential or to a transpassive potential were evaluated and correlate to passive film growth. Ex-situ XPS analysis was also performed to evaluate the chemical composition and the thickness of the passive film. By calibrating frequency to mass, it is possible to make a quantitative comparison between EQCM and XPS data.

Experimental

Quartz crystals.— AT-cut 10MHz quartz crystals (X-tronix, Switzerland) are used for the EQCM studies served as substrates for depositing the electrodes. The crystals were built up from plates quartz of 14 mm in diameter and 167 μm in thickness.[37] These crystals contained a thin film electrode on the back side formed by two layers, one of gold (with a thickness of 230 nm) and the second of chromium (20 nm) added to the crystal to improve adhesion. On the opposite side, a 1.45 μm thick CoCrMo layer was deposited by physical vapor deposition (PVD). The latter layer is simultaneously used to drive the crystal of an electric field and to act as working electrode in the electrochemical cell. Before the sputter deposition of the CoCrMo on the disk electrode, the quartz crystals were cleaned in an alkaline solution and degreased ultrasonically in iso-propanol for 15 minutes.

PVD depositions of CoCrMo layers on quartz crystals.— The PVD sputter deposition was carried out in an argon atmosphere using a magnetron Edwards ESM 100 PVD chamber equipped with a rotating sample holder. The target used was a Stellite 21 which composition was determined by X-Ray Fluorescence (Co 60.32%, Cr 33.84%, Mo 3.39%, Fe 1.42%, Ni 0.53%). The base pressure in the PVD chamber before admitting argon was 3.2 10^{-5} mbar, reaching a value of 10^{-2} mbar (pressure during deposition). During the CoCrMo deposition the sample holder was cooled with water with a refrigerant module adapted into the system. Before starting deposition, the substrate surface was cleaned by argon sputtering for 15 minutes. The used process parameters were: 500 V, 355 W, −200 V bias and 40 minutes of deposition time. The microstructure of the PVD deposits was observed using a JEOL 6300 F scanning electron microscope (SEM). Figure 1a shows that the PVD-coating is compact and dense with a fine-grain structure. The cross section of the Figure 1b shows that the film has a columnar structure with a thickness of 1.45 μm. This structure is related to the columnar growth mode of the deposit previously observed in other deposits of tungsten, stainless steel and chromium.[30,36,37]

To minimize interference with the anti-delamination Cr layer, the composition of the PVD layer was measured using EDX instead of XRF. Considering the different techniques used, the obtained coating composition (Co 64.87%, Cr 27.36%, Mo 5.37%, Fe 1.55%, Ni 0.00%, Si 0.85%) corresponds well with the target composition and in general

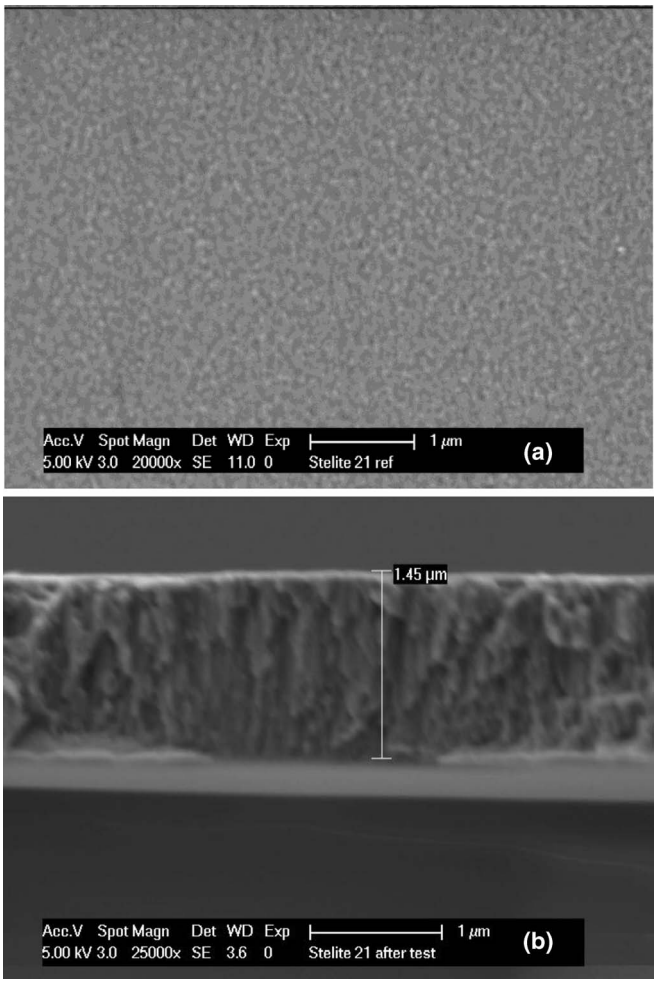

Figure 1. SEM images of the CoCrMo PVD deposits. (a) Surface and (b) cross sectional view after fracture.

with typical biomedical CoCrMo alloys. The presence of a weak Si signal in the coating is likely due to the quartz substrate.

In order to compare the polarization behavior of the coating to bulk alloys the polarization curve of the coating (see section 2.6) was graphically compared to published curves[43] in Figure 2. These curves were obtained with a single biomedical CoCrMo alloy in the same

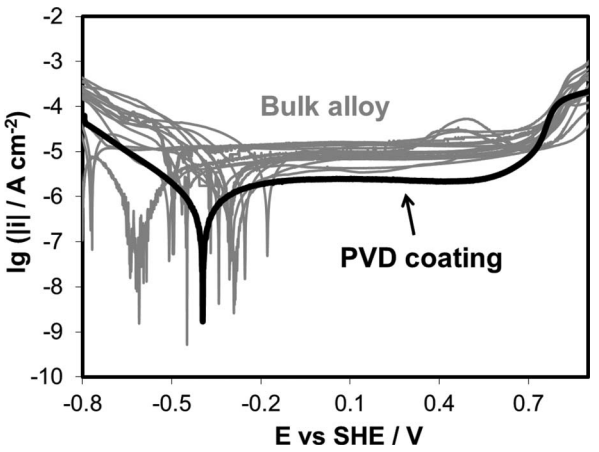

Figure 2. Comparison of polarization curves obtained with PVD-coating and using CoCrMo bulk alloys.

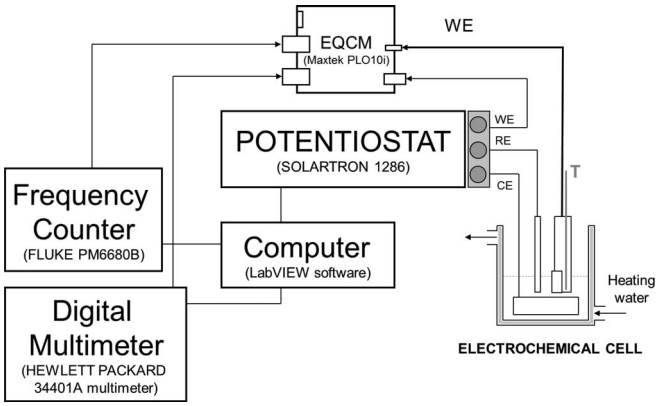

Figure 3. Schematic EQCM experimental setup.

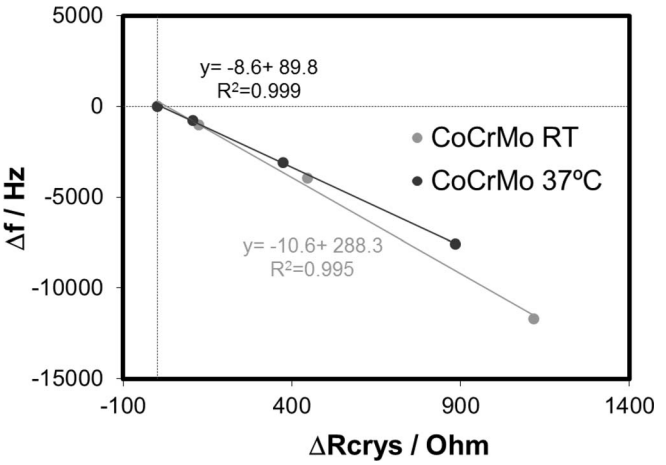

Figure 4. Variation of the resonant frequency of the quartz crystal electrode as a function of the crystal resistance for the CoCrMo alloy at room temperature and 37°C in solutions of different glycol/water concentrations.

solution that the presented one. The polarization curve of the PVD coating falls well within the scatter range of the published measurements. This indicates that the results obtained here with PVD coating are relevant for bulk alloys too.

Experimental cell set-up.— Figure 3 schematically shows the EQCM set-up. The oscillatory circuit used was a Maxtek PLO 10i connected to a Fluke PM6680B frequency counter and to a HP 34401 voltmeter (for measurement of the crystal resistance). The electrochemical conditions were controlled using a Schlumberger Solartron 1286 potentiostat. The entire measurement was controlled and data were logged through a National Instruments Labview interface.

A double walled three-electrode cell (volume 200 mL) was used for all the electrochemical measurements. An Ag/AgCl (3.5M KCl) reference electrode and a gold wire counter electrode were used. All potentials all given with respect to the Ag/AgCl electrode (SSE), the standard potential of which is 0.205 V with respect to the standard hydrogen electrode (SHE). The solution was not deareated and was kept at room temperature (24 ± 1°C) or at 37°C by circulating warm water between the two cell walls. Thus, to avoid thermal variations, related to the different temperature between the electrolyte and the back side of the quartz electrode, a stabilization time of around 30 minutes was imposed before starting the electrochemical experiments. Furthermore, a thermocouple introduced in the holder just behind the quartz crystal was used to verify that the temperature had reached a stable value within 30 minutes.

The electrolyte consisted of a pH 7.4 phosphate buffer solution (PBS) with the following composition: 0.14M NaCl, 1mM KH_2PO_4, 3mM KCl and 10mM Na_2HPO_4.

For the electrochemical experiments the quartz crystals were placed in a vertical Teflon holder previously described by Schmutz et al.[32] Care was taken to maintain the same height of the working electrode with respect to the electrolyte level in all tests since different hydrostatic pressure on the crystal surface may affect the EQCM measurements.

Correction constant for viscous loading.— Water/glycerol solutions with the concentrations of 100, 75, 50 and 25% (in water volume) were prepared in order to determine the proportionality constant (K) that allows one to correct the total frequency for viscous loading (equation 3). These solutions are chemically inert and do not lead to absorption on the metal surface and therefore Δf_m can be neglected.[28,44] Thus, the change in frequency is only related to the viscous load.

Figure 4 shows the frequency variation (Δf) and the variation of the crystal resistance (ΔR_{crys}) with respect to pure water after immersion of the crystal in the glycerol solutions. A good linear dependence is found in agreement with equation 3. The slopes of the linear interpolations give K values of −10.6 and −8.6 Hz Ω^{-1} for room temperature and 37°C, respectively.

Calibration of the Sauerbrey constant.— The quartz sensitivity factor (C_f) in the Sauerbrey equation can be calculated theoretically or measured experimentally. The theoretical values of the C_f can be obtained using the physical properties of the crystal, however the experimental method obtained by the electrodeposition of copper on a gold electrode at 100% current efficiency gives more accurate C_f values.[28] This latter approach was used in this work.

Copper was plated from a solution of 0.5M $CuSO_4$ + 0.5M H_2SO_4 + 1.1M ethanol at room temperature and 37°C at an applied potential of $-0.21V_{Ag/AgCl}$. Previous studies showed that this electrolyte show a current efficiency of 100% at this cathodic potential.[45,46] The current density j and the frequency change Δf due to the electrodeposition were registered during the test (Figure 5). The contribution of viscous loading was subtracted using the constant described above. The Sauerbrey constant C_f was determined using equation 4:

$$C_f = -\frac{\Delta f_m}{\Delta m} = -\frac{\Delta f_m}{\frac{q \cdot M_{Cu}}{n \cdot F}} \cdot a_{cond} \qquad [4]$$

where q is the electrical charge (integrated from the current vs time curves as shown in Figure 5), M_{Cu} is the atomic mass of copper (63.54 g mol^{-1}), n is the charge number or valence of dissolution of the metal (2 in this case), F is the Faraday constant (96485 C mol^{-1}) and a_{cond} is the conductive area in cm^2 (23.13 cm^2).

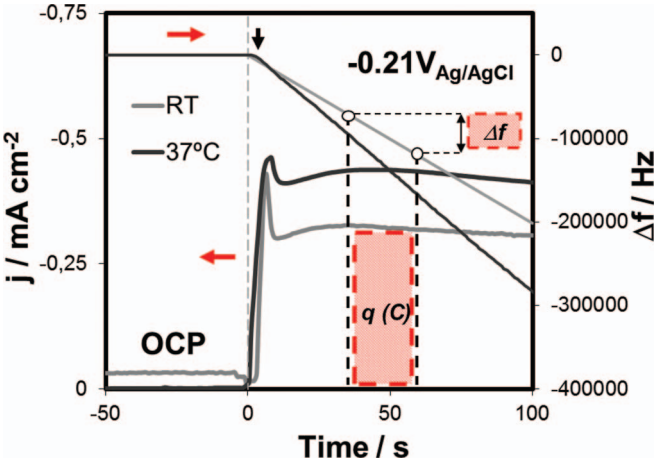

Figure 5. Current and frequency evolution obtained during the electrodeposition ($-0.21V_{Ag/AgCl}$) of copper on a gold electrode at room temperature (RT) and 37°C.

The experimental values of the sensitivity factor (C_f) are 0.20 ± 0.05 and 0.21 ± 0.01 Hz cm^2 ng^{-1} at room temperature and 37°C, respectively (average values of 3 independent tests for each temperature). Therefore, at lower temperatures, the same change in frequency corresponds to higher variation in mass on the electrode surface.

EQCM measurements on CoCrMo.— Two different electrochemical tests were conducted with the described EQCM set-up: potentiodynamic curves and potential step tests.

The general corrosion behavior of the CoCrMo alloy was analyzed by potentiodynamic measurements. Initially, open circuit was measured for 10 min. The scans were started at a cathodic potential of -1 $V_{Ag/AgCl}$ and moved into the anodic direction up to the transpassive region (limited at a maximum current of 200 mA) at a scan rate of 1mV s^{-1}. Current response and frequency were simultaneously measured during the scan. The potentidynamic curves were carried out in the following experimental conditions: (a) PBS at room temperature and (b) PBS at 37°C. All experiments were carried out under non deaerated conditions. The corrosion potential (E_{corr}) as well as the passive current density (i_p) and the breakdown potential (E_b) were extracted from the polarization curves. The i_p was obtained at the passive potential of 0.1 $V_{Ag/AgCl}$.

On the other hand, the film growth of the CoCrMo was analyzed potentiostatically using potential steps experiments (passivation experiments). These tests consisted in maintaining the potential at -0.05 $V_{Ag/AgCl}$ for 30 minutes and subsequently increasing it at a fast controlled scan rate (10 and 100 mV s^{-1}) to 0.35 or 0.55 $V_{Ag/AgCl}$. The sample is kept at this potential for 30 minutes. The response in current and frequency is monitored all along the test. Before the test, the open circuit potential was measured for 10 min. The use of different potential scan rates allows one to investigate the film response of the alloy to a potential change.[36] Furthermore, potential step tests from OCP to -0.05 $V_{Ag/AgCl}$ were also performed.

X-ray photoelectron spectroscopy.— After the electrochemical experiments the samples were taken out of the cell with the polarization switched on. They were rinsed with water and blow-dry with nitrogen before being stored in a dessicator for at least one week before XPS analysis.

Table I. XPS peaks considered for fitting.

Element	Peak	Oxidation state	Binding Energy
Cr	$2p_{2/3}$	Cr	573.8 ± 0.4
		Cr^{+3} oxide	+2.2
		Cr^{+3} hydroxide	+3.4
		Cr^{+6}	+4.9
Co	$2p_{2/3}$	Co	778 ± 0.6
		Co oxidized	+2.5
Mo	$3d_{5/2}$	Mo	227.5 ± 0.3
		Mo^{+4} oxide	+1.5
		Mo^{+4} hydroxide	+3.4
		Mo^{+6}	+4.9
O	1s	O^{2-}	530.2 ± 0.7
		OH^-	+1.6
		H_2O	+3.0

The XPS measurements were performed with a Kratos AXIS ultrahigh resolution spectrometer, using a monochromatic Al K_α X-ray source and a take-off angle of 0° with respect to the surface normal. No sputtering was performed prior to analysis. The energy scale was calibrated by fixing the adventitious carbon peak 285 eV. The fitting of the XPS-spectra was performed using the commercial software package CasaXPS and the peaks listed in Table I. The evaluation procedure included an iterated Shirley procedure for background subtraction. The peak identification was made to obtain a consistent fit at all the investigated potentials. The metal peak positions were allowed to float to compensate for a slight charging in the passive film. For quantification, relative sensitivity factors given by the XPS instrument supplier were used. The passive film thickness was calculated using the intensity ratios of oxidized metal over the metallic signal. The passive film was divided into an oxide and a covering hydroxide-water layer according to a method used previously.[5,6,37,47–49]

Results

Potentiodynamic curves.— Figure 6 shows the current density evolution and the mass change represented in function of the potential sweep carried out in PBS (a) at room temperature and (b) at 37°C.

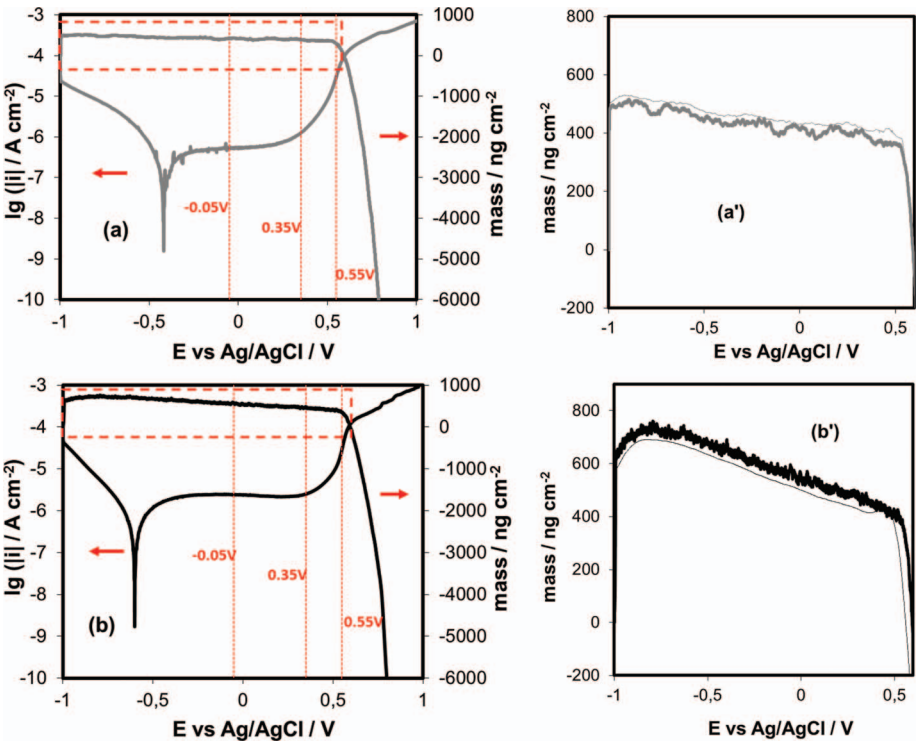

Figure 6. Potentiodynamic curve and simultaneous measurement of mass change of the CoCrMo alloy at 1mV/sec in PBS (a) at room temperature and (b) 37°C. Figure 5(a′) and 5(b′) show the enlargement of the mass variation in the active and passive domains.

Table II. Electrochemical parameters of the CoCrMo alloy in simulated body fluids at different conditions.

Electrolyte	Temperature	E_{corr} ($mV_{Ag/AgCl}$)	i_p ($\mu A/cm^2$)	E_b ($mV_{Ag/AgCl}$)
PBS	Room Temperature	-418 ± 10	0.51 ± 0.22	389 ± 35
PBS	37°C	-600 ± 54	2.38 ± 0.18	471 ± 21

After the correction for viscous loading, the mass signal was smoothed using a Savitzky-Golay algorithm.[50]

The cathodic domain below -0.5 $V_{Ag/AgCl}$ is characterized by a negative current density due to the reduction of dissolved oxygen and partially of water. In this domain, the mass increases significantly at the beginning of the tests in particular at 37°C. Indeed, the maximum value of mass reached at 37°C was 760 ng cm^{-2} (at -0.8 $V_{Ag/AgCl}$) while at room temperature only a maximum of 500 ng cm^{-2} (at -0.9 $V_{Ag/AgCl}$) was observed. The continuous and slight increase of the mass in this cathodic domain is clearly observed in the enlargements of the mass variation versus potential between -1V and 0.6 $V_{Ag/AgCl}$ represented in Figure 6(a′) and 6(b′). This mass increase is likely related to the build up of an oxide film on the CoCrMo alloy surface, which interestingly occurs at relatively large cathodic potentials. However, other phenomena such as adsorption could contribute to the mass increase.

The second domain corresponds to the passive plateau which extends over a broad range of potentials (from -0.4 to 0.4 $V_{Ag/AgCl}$ approximately). In this domain, the current density remains constant and monotonic loss of mass is observed. This behavior corresponds well to passive dissolution.

The transpassive domain can be divided in two regions: the first from approximately 0.4 to 0.6 $V_{Ag/AgCl}$ and the second from 0.6 to 1 $V_{Ag/AgCl}$. The first transpassive region (I) is characterized by an abrupt increase in the current density at approximately 0.4 $V_{Ag/AgCl}$ without any significant change in mass loss rate. This potential lies in between the equilibrium potentials of the oxidation of Cr(III) to Cr(VI) (0.2 $V_{Ag/AgCl}$) and of the water oxidation (0.6 $V_{Ag/AgCl}$). Therefore this current increase can be attributed to the formation of Cr(VI).

On the other hand, in the second transpassive region (II), a strong decrease of the mass takes place above 0.6 V due to transpassive dissolution.[5] This potential corresponds to the reversible potential of water and to a change in anodic kinetics characterized by a shoulder in the polarization curve.

Similar transpassive behavior was reported in a previous EQCM investigation of FeCr alloys in sulphuric acid solutions.[33] This and the present findings indicate that oxidation of Cr(III) to Cr(VI) is not sufficient to trigger transpassive dissolution.

Table II summarizes the electrochemical parameters E_{corr}, i_p and E_b extracted from the potentiodynamic curves. At 37°C these characteristic values correspond well with the average values obtained under similar conditions in a round robin test carried out using Co28Cr6Mo bulk alloys.[43] Clearly those parameters are significantly affected by the temperature which shifts E_{corr} toward lower values and increases i_p one order of magnitude. The temperature also influences the measured mass loss. At room temperature (Figure 6a) the mass reached a maximum value of 500 ng cm^{-2} while a 37°C (Figure 6b) the maximum is 760 ng cm^{-2}. This indicates that passive film thickness increases with temperature. Furthermore, temperature accelerated passive dissolution of the CoCrMo alloys. Indeed, the slope of the mass vs potential curves (Figure 6(a′) and Figure 6(b′)) in the passive domain raises from 100 ng cm^{-2} V^{-1} at room temperature to 260 ng cm^{-2} V^{-1} at 37°C.

Potential step measurements.— Potentiostatic tests were performed in order to characterize the passive film growth. The following experimental variables were investigated: scan rate, temperature and passive and transpassive potential. The Figure 7 shows the experimental results obtained in PBS during the potential step from -0.05 to 0.35 $V_{Ag/AgCl}$ (a) at the scan rates of 10mV/s at room temperature, (b) at the scan rate of 10mV/s at 37°C and (c) at the scan rate of 100mV/s at 37°C. The results obtained during the potential step test from -0.05 to 0.55 $V_{Ag/AgCl}$ in PBS at 10mV/s at room temperature and 37°C has been plotted in Figure 8. The selected potentials correspond to the passive (0.35$V_{Ag/AgCl}$) and in region (I) of the transpassive domain (0.55$V_{Ag/AgCl}$). The total frequency was measured simultaneously to the total current density. Thus, after correcting the total frequency for viscous loading and after applying the Sauerbrey equation (equation 2) the variation of the total mass measured by the EQCM was obtained ($mass_{EQCM}$).

Figures 7b and 7c show the response of the current density when two different scan rates were used. The peak current is higher at 100 mV s^{-1} scan rate but the steady-state current density after approximately 500 s (0.9 μA cm^{-2}) as well as the total charge (3.1 ± 0.3 and 2.8 ± 0.2 mC cm^{-2} for 10 and 100 mV s^{-1} respectively) are little affected by scan rate. Figure 7(b′) and 7(c′) show the evolution of the mass variation measured during the potential step test carried out at 0.35 $V_{Ag/AgCl}$ at different scan rates. The mass evolution shows a continuous loss (passive dissolution) until approximately 900 s when the mass change reaches a steady-state plateau. The plateau values are 216 ± 4 and 175 ± 10 ng cm^{-2} for the 10 and 100 mV s^{-1} of scan rates, respectively. This difference suggests faster passivation at higher scan rate thus yielding less dissolution. The fact that the steady-state is reached earlier at higher scan rate support this hypothesis, Figures 7(b′) and 7(c′).

Figures 7(a-a′) and 7(b-b′) show the effect of temperature on passive film growth. While temperature does not affect the shape of the current transient it influences the total charge and the mass loss. In fact, at room temperature the mass loss in the steady state (174 ± 5 ng cm^{-2}) is lower than at 37°C (216 ± 4 ng cm^{-2}) while the charge changes from 1.8 ± 0.3 mC cm^{-2} (room temperature) to 2.9 ± 0.3 mC cm^{-2} (37°C).

The response of the current density and the $mass_{EQCM}$ at the applied potential step from -0.05 to 0.55 $V_{Ag/AgCl}$ (transpassive domain) at room temperature and 37°C is represented in Figure 8. After an initial peak the current stabilizes after approximately 300 s at values of 32.2 and 50.3 μA cm^{-2} at room temperature and 37°C, respectively. A similar transient behavior was observed by Hodgson et al.[5] on bulk CoCrMo samples passivated at the same potential in buffered 0.14M NaCl solution. In addition, in the Figure 8(a′), the evolution of the mass loss measured by the EQCM shows a straight line with time. The final mass loss is 8 ± 0.7 μg cm^{-2} at room temperature and 12 ± 2.5 μg cm^{-2} at 37°C. The mass loss at 0.55 $V_{Ag/AgCl}$ is much larger than at passive potential due to transpassive dissolution that is apparently accelerated at higher temperature. At this potential, a direct dependence of the $mass_{EQCM}$ and the charge is obtained, according to the Faraday's law, obtaining an overall value of n of 4.3. This confirms that the dissolution rate increases due to the dissolution of Cr(VI), Co(III) and Mo(VI) species.

XPS analysis.— The XPS measurements were used for determining the chemical composition of the passive film, the atomic concentration of the species presents in the oxide film and in the bulk metal and finally, the oxide film thickness. Thus, XPS analysis was performed on samples after the potentiostatic tests under the different experimental conditions. In addition, the XPS spectrum was also obtained for the sample polarized after the first step potential (from OCP to -0.05 $V_{Ag/AgCl}$) for analyzing the variation in thickness and composition between the first and the second potential step (from -0.05 to 0.35 $V_{Ag/AgCl}$ and from -0.05 to 0.55 $V_{Ag/AgCl}$).

The peaks of the alloying elements were deconvoluted according to metallic and oxidized species (Table I). Figure 9 shows an example of the deconvolution of (a) cobalt (Co2p), (b) chromium (Cr2p) and (c) molybdenum (Mo3d) in a sample measured after potentiostatic step from -0.05 to 0.35 $V_{Ag/AgCl}$ at the scan rate of 10mV/s at 37°C. While the oxidized state significantly contributes to the Cr and Mo

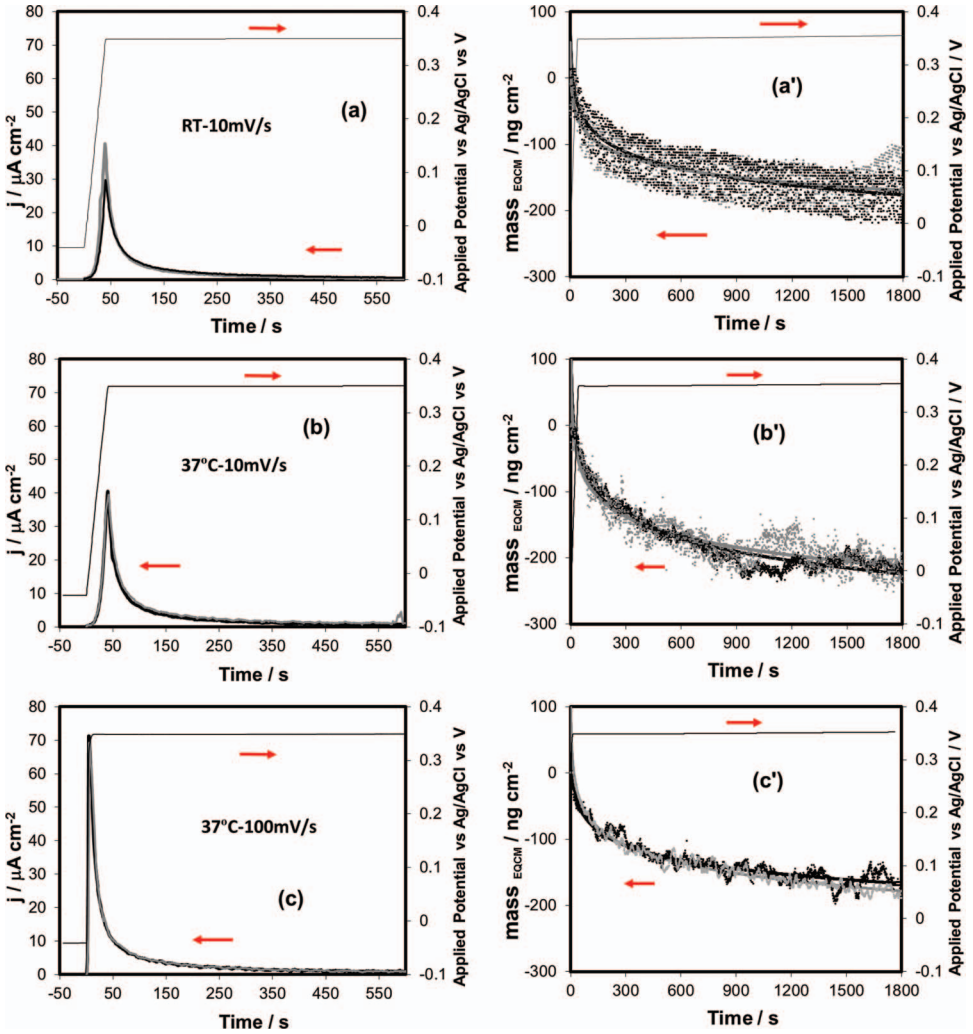

Figure 7. Current density evolution (left) and mass change (right) measured by the EQCM (m_{EQCM}) in potential step tests from −0.05 to 0.35 $V_{Ag/AgCl}$ of a CoCrMo biomedical alloy in PBS (a-a′) at room temperature and 10 mV/s, (b-b′) at 37°C and 10 mV/s and (c-c′) at 37°C and 100 mV/s. Results from two independent tests are shown. Continuous lines in the right corresponds to exponential interpolation of the measurements points.

signals its contribution to the Co spectrum is very small. All samples suffered carbon adventitious contamination as indicated by the large C peaks situated at 285 eV. On all samples a weak P signal was observed with the maximum intensity at approximately 134 eV indicating the presence of phosphate ions. Adsorption of phosphates from simulated body fluids on the CoCrMo passive films was already reported in the literature.[6,51] The three states O_2^-, OH^- and H_2O contributed the O (O1s) peak (Figure 10).

The approach developed by Olsson and Landolt[5,47] for characterizing passive films formed in simulated body fluids on CoCrMo alloy was used here for XPS quantification. This approach assumes a four layered structure of the passive surface involving an adsorbed

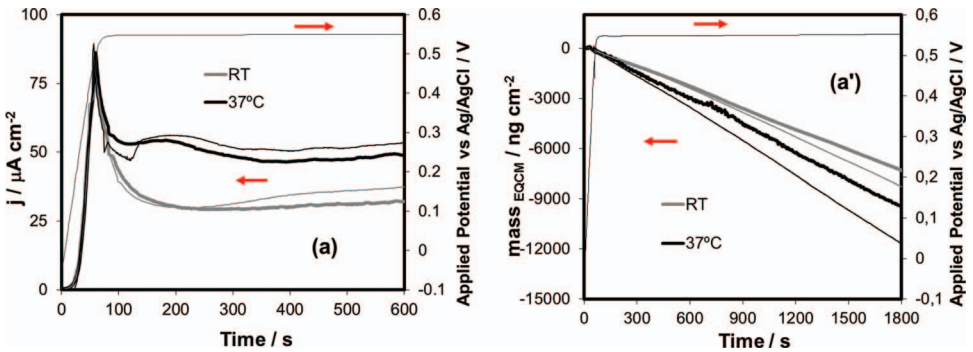

Figure 8. (a) Current density evolution and (a′) mass change measured by the EQCM (m_{EQCM}) in potential step tests from −0.05 to 0.55 $V_{Ag/AgCl}$ of a CoCrMo biomedical alloy at 10 mV/s in PBS at room temperature and 37°C. Two independent tests are shown for each condition.

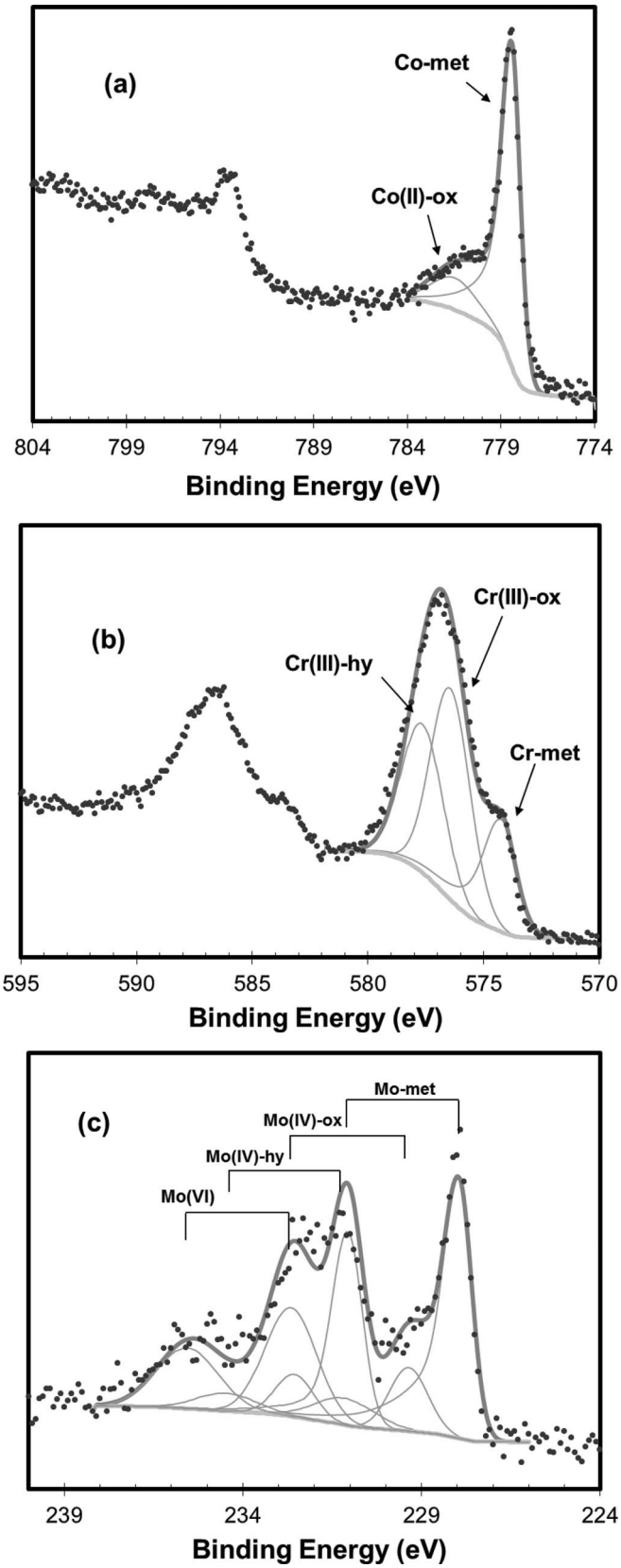

Figure 9. XPS spectra and the corresponding fitted peaks measured on the CoCrMo alloy after the potential step test from −0.05 to 0.35 $V_{Ag/AgCl}$ at 10 mV/s in PBS at 37°C: (a) cobalt, (b) chromium and (c) molybdenum.

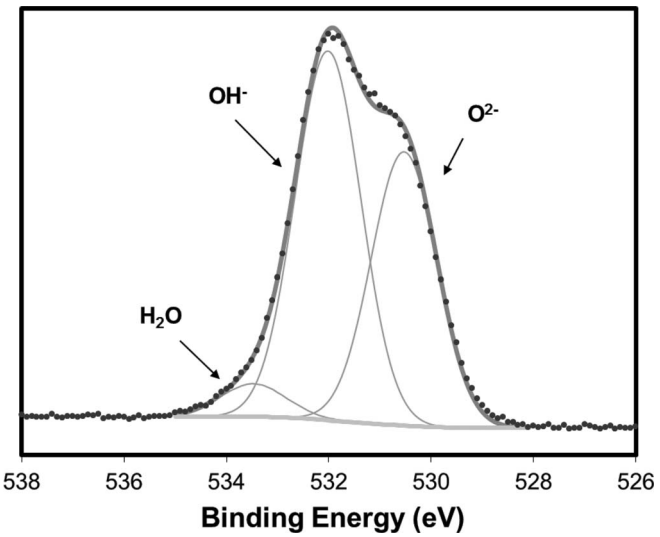

Figure 10. XPS oxygen spectrum and corresponding fitted peaks for the CoCrMo alloy after the potential step test from −0.05 to 0.35 $V_{Ag/AgCl}$ at 10 mV/s in PBS at 37°C.

water film, an outermost hydroxide film, an internal oxide film and the underlying metal. By this method it is possible to calculate film thicknesses and atomic concentration from the deconvoluted peaks areas as well from the values of inelastic mean free paths (IMFPs) which was calculated using TPP2 equation[52,53] and from sensitivity factor given by the XPS instrument manufacturer ($Co2p^{2/3}$ 2.362, $Cr2p^{2/3}$ 1.583, $Mo3d^{5/2}$ 2.005, C1s 0.278, O1s 0.780).

The calculated film thicknesses listed in Table III are in good agreement with previously obtained results.[4–6] In all cases the water film is very thin (less than one monomolecular layer) and therefore was not further considered here. Thus, the passive film was considered to consist of the hydroxide layer and oxide layer only. The ratio between hydroxide and oxide film thickness is about 1:1 for passive potentials and 2:1 for the transpassive potential. The thickness obtained at transpassive potentials is much larger than in the passive domain. This is consistent with previous works.[4,5] The scan rate has no noticeable effect while films forms at 37°C are slightly thicker than the ones formed at room temperature.

The atomic concentration ratios of the elements Co, Cr and Mo in their oxidized state in the passive film, determined by deconvolution of the XPS spectra, are plotted in Figure 11. Temperature and scan rate have no significant effect on the composition of the passive film. In the passive domain the passive film mainly contains Cr(III) ions and its cobalt content decreases with increasing potential. In the transpassive domain Co constitutes more than 50% of the cations and a significant fraction of Cr ions are oxidized to the valence VI. The present XPS analyzes are in good quantitative and qualitative agreement with literature results obtained on bulk CoCrMo alloys.[4–6,54]

Discussion

Film growth in the passive domain.— The current density peak obtained at the beginning of the anodic polarization (Figure 7) indicates high metal dissolution, exceeding the oxygen incorporation into the growing film, i.e. only a fraction of the cations formed at the metal/film interface contributes to film growth while the rest becomes dissolved in the solution. This behavior was also observed working with stainless steel.[32,55] According to the results shown in Figure 7 the balance in the film/electrolyte interface, $mass_{EQCM}$, is characterized by the dissolution of the cations through the passive film into the electrolyte. These results are in good agreement with the mass variation obtained in the passive domain of the polarization curves (Figure 6). In those tests a decrease in mass was observed during passivation;

Table III. Film thicknesses calculated by the convolution of the XPS peaks of the different alloying elements at different applied potentials and scan rates of the CoCrMo alloy in PBS at room temperature and 37°C.

				Thickness (nm)			
First Step	Second Step	Temperature	Scan rate (mV/s)	Oxide	Hydroxide	Water	Passive film[a]
OCP	−0.05 V	RT	10	0.9	0.7	0.1	1.6
				1.0	0.6	0.0	1.6
OCP	−0.05 V	37°C	10	0.9	0.7	0.2	1.6
				0.9	0.7	0.1	1.6
−0.05 V	0.35 V	RT	10	1.2	1.1	0.0	2.3
				1.2	1.1	0.1	2.3
−0.05 V	0.35 V	37°C	10	1.3	1.2	0.1	2.5
				1.1	1.2	0.1	2.4
−0.05 V	0.35 V	37°C	100	2.4	1.4	1.0	2.4
				2.3	0.8	1.5	2.3
−0.05 V	0.55 V	RT	10	4.8	3.1	0.0	7.8
				7.2	2.3	0.1	9.5
−0.05 V	0.55 V	37°C	10	5.0	2.8	0.2	7.8
				11.8	2.9	0.2	14.6

[a] Oxide + Hydroxide.

however, the mass that goes to the film growth, $mass_{FILM}$, is expected to increase with time.

The *passive film growth* can be correlated with the mass changes taking place at the electrode surface which are determined by the concurrent phenomena of passive film growth and passive dissolution. A procedure for the quantitative appraisal of these phenomena results has been developed previously.[31,36,37] This procedure has been applied in the present study.

Figure 12 shows the mass balance of the ions implicated in the oxide film formation of the CoCrMo alloy. According to this representation all mass change going into the oxide film, through the interface metal/film (interface denoted as I) and film/electrolyte (interface II) are considered positive. Therefore, the incorporation of cations and anions into the passive film corresponds to a positive mass change. The negative mass change is due to ions moving from the oxide film to the electrolyte.

Three assumptions were made to interpret the EQCM data (*i*) all elements are oxidized corresponding to their relative bulk concentration at the metal-film interface, (*ii*) the cations remaining in the film have the same oxidation number as when they are first oxidized and *(iii)* only O^{2-} and OH^- anions were considered.

Thus, the film thickness change has been calculated using the equation 5 which is adapted for the CoCrMo alloy according to previous works[36]:

$$\Delta m_{tot}^{film} = \sum_{i=cation} \Delta m_i^I + \Delta m^{EQCM} \quad [5]$$

where Δm_i^I denotes the mass change for each cation of the alloying elements through the metal/oxide interface (I) and the Δm^{EQCM} is the mass change at the film/solution interface (II) which is measured by the EQCM. The latter parameter includes the contribution of the cations (Co, Cr and Mo) and the oxygen (needed for oxide formation) from the electrolyte (Figure 12).

The Δm_i^I values for each cation is determined by Faraday's law (equation 6):

$$\Delta m_i^I = \frac{q_i M_i}{n_i F} \quad [6]$$

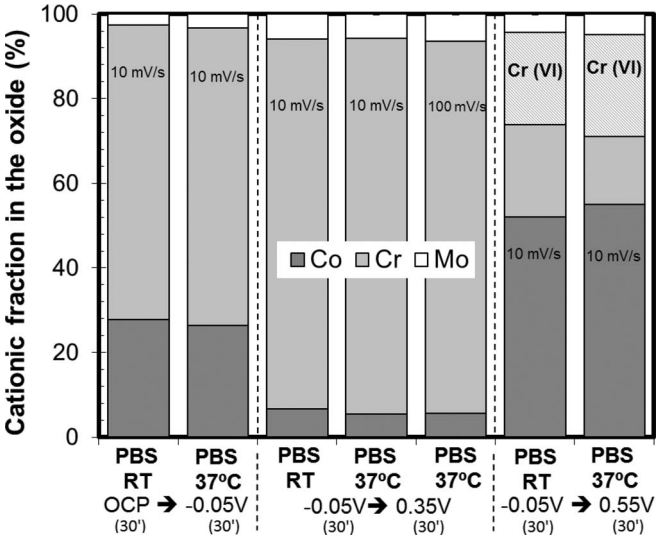

Figure 11. Cationic fraction in the oxide film as measured by XPS at different applied potentials and scan rates of the CoCrMo alloy in PBS at room temperature and 37°C.

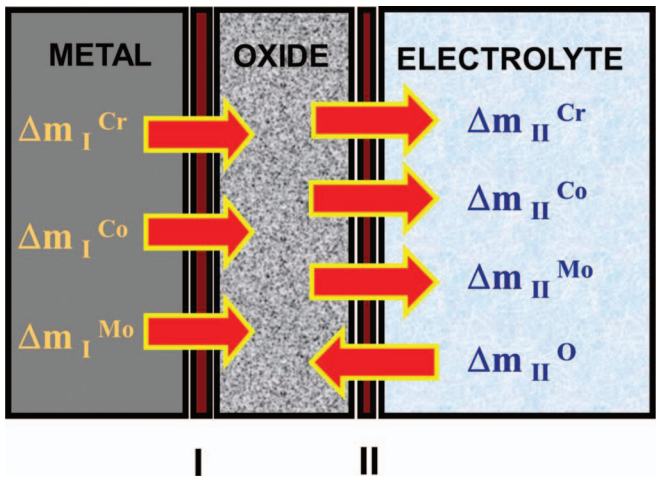

Figure 12. Mass flow convection of the metals that contributes to the oxide film formation. The sign is positive for the flows that favor the film formation through the interfaces I and II.

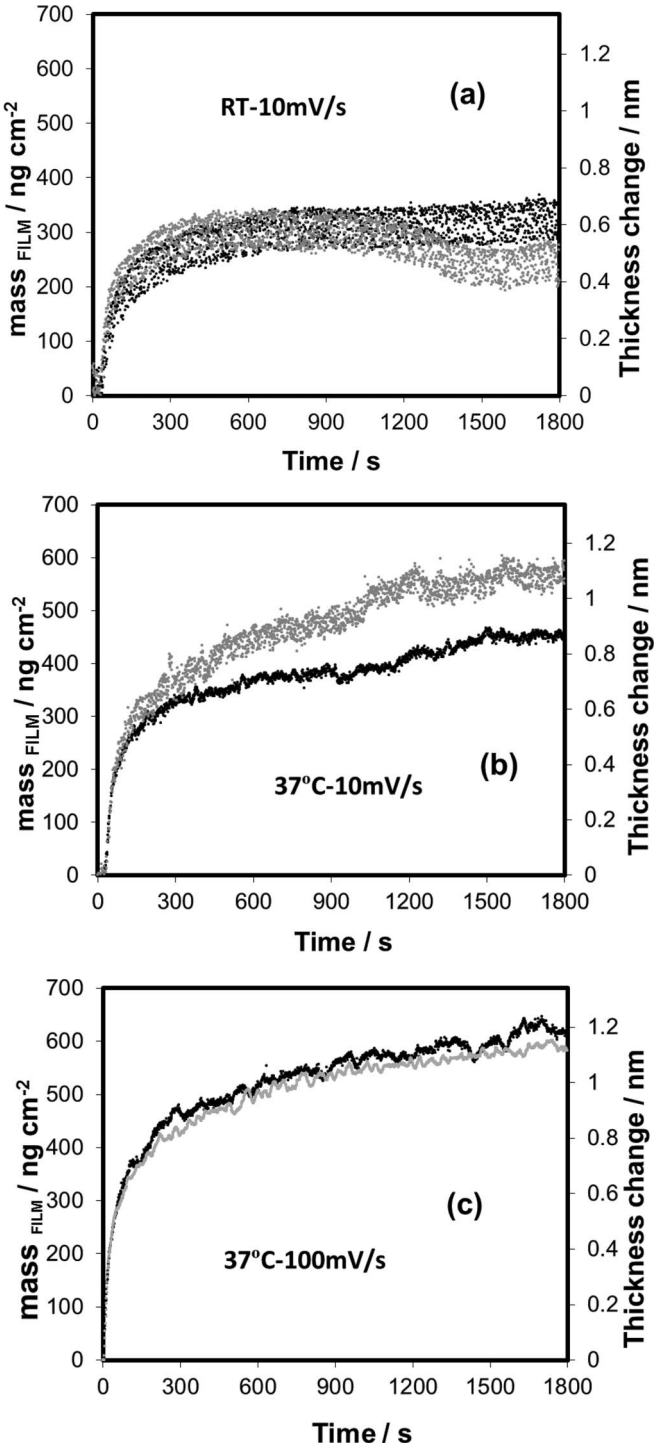

Figure 13. Total mass change (m_{FILM}) and thickness change (calculated by dividing the former parameter by the film density) of the film during passivation CoCrMo in PBS from −0.05 to 0.35 $V_{Ag/AgCl}$ (a) at 10 mV/s at room temperature, (b) at 10 mV/s at 37°C and (c) at 100 mV/s at 37°C. Results from two independent tests are shown.

where q_i is the charge density, M_i is the molar mass of the element i, F is the Faraday's constant, n_i is the valency, and c_i is the bulk atomic concentration of the element i.

The mass variation of the oxide film ($mass_{FILM}$) extracted from equation 5 has been represented in Figure 13. The change of the *thickness* of the passive film can be calculated by dividing the film mass change by the average film density ρ(g cm^{-3}). The evolution of the film thickness with time is also illustrated in Figure 13.

During passivation at 0.35 $V_{Ag/AgCl}$ the film grows initially (first 100 seconds) very fast. Afterwards the growth rate decreases progressively. Finally the film thickness reaches a plateau value after 600 s at room temperature or 1500 s at 37°C. The scan rate does not significantly affect the growth kinetics. The increase in film thickness due to passivation at 0.35 $V_{Ag/AgCl}$ was extracted from Figure 13 for each experiment and listed in Table IV together with the corresponding XPS values. The latter was determined by subtracting the total thickness (oxide+hydroxide) of the film formed at −0.05 $V_{Ag/AgCl}$ to the thickness of the passive films formed at 0.35 $V_{Ag/AgCl}$ (Table III). Taking into account the uncertainties associated with EQCM measurements and XPS quantification (errors in peak fitting and calculation of electron means free path) the results of Table IV show a good correlation between the two techniques. Both EQCM and XPS indicate that the passive film grown at room temperature is slightly thinner that the one forming at 37°C.

These results (Figure 7 and Figure 13) clearly indicate that the potentiostatic passivation process is characterized by a continuous loss of mass through the film/electrolyte interface accompanied by film growth.

Film growth in the transpassive domain.— The same film growth quantification procedure described in the previous section was applied to the potentiostatic test carried out at the transpassive potential of 0.55 $V_{Ag/AgCl}$. The obtained film growth kinetics are shown in Figure 14 at room temperature and 37°C. At both temperatures the film thickness increases linearly with time. The average growth rate is 0.49 ± 0.05 and 0.77 ± 0.06 nm min^{-1} at room temperature and 37°C respectively, i.e. being faster at higher temperature. The Figure 8 shows that the current reaches a constant value soon after polarization despite the continuous growth of the oxide film. Thus the oxidation kinetics is apparently not influenced by the oxide film. Such situation typically arises when surface films are cracked or porous.

The thickness change as measured by EQCM is very reproducible and corresponds to average values of 15 and 25 nm for room temperature and 37°C respectively (Table IV). Interestingly XPS yields much lower values and significant scattering particularly at 37°C. These differences between the two techniques may be due to several reasons. First XPS being an ex-situ technique, film thinning can occur during sample rinsing with water after polarization. The thinning is not necessarily uniform which could result in variations of film thickness measured by XPS depending on location of the analyzed area on the sample surface. Furthermore, thick surfaces films attenuate the

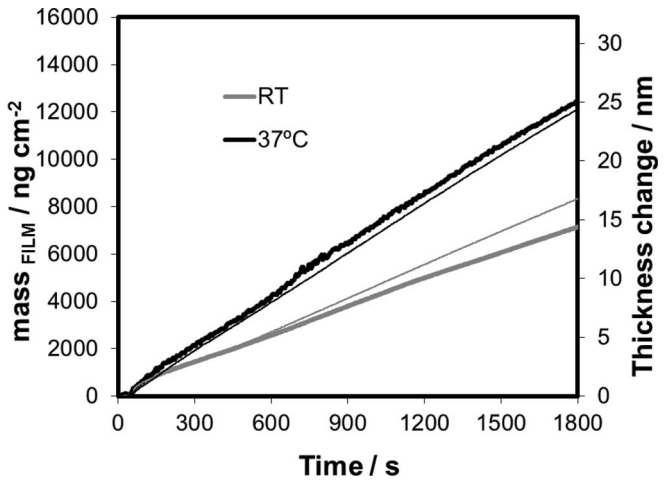

Figure 14. Total mass change (m_{FILM}) and thickness change of the film during transpassive polarization of CoCrMo in PBS from −0.05 to 0.55 $V_{Ag/AgCl}$ at 10 mV/s at room temperature and 37°C.

Table IV. Film thickness change obtained in the second potential step determined by EQCM and XPS (obtained subtracting to the total thickness the obtained after the first potentiostatic step) of the CoCrMo alloy at different scan rates and temperatures.

				Thickness Change (nm)	
First Step	Second Step	Temperature	Scan rate (mV/s)	EQCM	XPS
−0.05 V	0.35 V	RT	10	0.6	0.7
				0.5	0.7
−0.05 V	0.35 V	37°C	10	0.9	0.9
				1.0	0.8
−0.05 V	0.35 V	37°C	100	1.2	0.8
				1.1	0.8
−0.05 V	0.55 V	RT	10	14.7	6.2
				16.5	7.9
−0.05 V	0.55 V	37°C	10	25.9	6.2
				23.9	13.0

XPS metallic signal down to very low, difficult to quantify intensities. This uncertainty may affect the outcome and scattering of XPS quantification. The present results show that EQCM, thanks to its in situ character, can constitute an extremely valid alternative to XPS for studying film thicknesses.

Transpassive oxidation and dissolution of the CoCrMo alloy.— In the measured EQCM polarization curves (Figure 6) the potential (transpassive oxidation potential) at which the current start to increase after the passive potential does not match the potential at which mass loss starts increasing (transpassive dissolution potential). In order to illustrate this, the derivative of the mass with respect to time during the polarization curve was calculated and plotted together with the current in Figure 15.

This figure shows that up to the potential of 0.52 $V_{Ag/AgCl}$ the dissolution rate is negligible. Above this potential the dissolution rate abruptly increases. Thus the potential 0.52 $V_{Ag/AgCl}$ can be defined as the transpassive dissolution potential (E_{TD}). Up to this potential the passive state is maintained. However, the transpassive oxidation potential (E_{TO}) corresponding to the oxidation of Cr(III) to Cr(VI) occurs at a lower potential (0.28 $V_{Ag/AgCl}$) as indicated by the current curve. This indicates that Cr(VI) ions can form in the passive film of CoCrMo alloy without affecting passive dissolution. Similar results were found by Schmuki et al.[56] when investigating transpassivity of Cr_2O_3 films using in-situ X-Ray Near-Edge Spectroscopy combined with electrochemical techniques. They detected the presence of Cr(VI) at passive potentials and concluded that Cr(VI) is incorporated in the Cr_2O_3 prior to transpassive dissolution. The factors responsible for triggering the transpassive dissolution are not clear at present. According to Schmuki et al.[56] formation of chromate ions occurs within the film by reaction of Cr(VI) ions with inwards diffusing oxygen anions. Transpassive dissolution starts only when a critical concentration of chromate ions is reached at the oxide surface. Based on this hypothesis one could conclude that sufficient chromate ions formed on the CoCrMo passive film only above E_{TD} (0.52 $V_{Ag/AgCl}$). However, this ignores possible influences by Co and Mo ions which cationic fraction increases significantly close to the transpassive potential of CoCrMo alloys.[4,5]

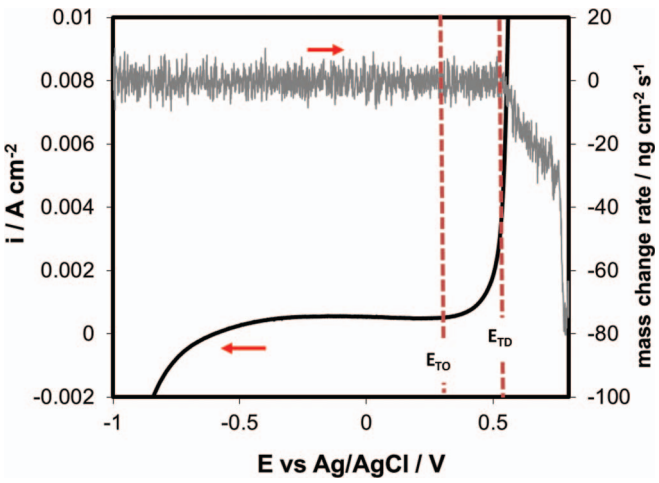

Figure 15. Current density and derivative of the mass with respect to time during the polarization curve of the CoCrMo alloy at 1mV/sec and 37°C in PBS.

Influence of temperature on mass and thickness change.— The results in Figure 6 show that temperature affects the passive dissolution (potentials below E_{TD}) but neither oxidation of Cr(III) to Cr(VI) nor transpassive dissolution (for potentials larger than E_{TD}). This is in agreement with previous results showing an increase in corrosion rate of CoCrMo alloys with increasing temperature.[57]

On the other hand, the increase in temperature also enhances the oxide film thickness (0.3–0.4 and 0.12–0.1nm with EQCM and XPS respectively) in the potentiostatic tests carried out at 0.35 $V_{Ag/AgCl}$, Table IV. This indicates that despite their larger thickness passive films formed at 37°C are less protective than the ones form at lower temperature. These results demonstrate the need of controlling temperature for the study of the electrochemical processes occurring on biomedical alloys such as the CoCrMo alloy in biological systems. EQCM results obtained at room temperatures may underestimate the kinetics of the film growth and passive dissolution.

Conclusions

Combined EQCM and XPS experiments have been used for analyzing the electrochemical behavior of a PVD-CoCrMo biomedical alloy in phosphate buffer solution at 37°C. The simultaneous measurements of the electrode mass change in the nanogram range, of the current and charge permitted, using the passive film composition determined by XPS, the evaluation of the passive film growth and passive dissolution kinetics. The following conclusions are drawn:

- The electrochemical behavior of the PVD-CoCrMo alloy corresponds well with the one observed for the CoCrMo bulk alloy.
- All over the potential range investigated, mass loss was observed. In the passive region, mass loss was considerably lower than in the transpassive region. Increasing temperature promotes passive and transpassive dissolution.
- In potentiostatic tests at 0.35 $V_{Ag/AgCl}$ (passive potential) the passive film initially grows at a fast rate of over 0.25 nm min^{-1} (room temperature and 10 mV s^{-1}), 0.33 nm min^{-1} (37°C and 10 mV s^{-1}) and 0.57 nm min^{-1} (37°C and 100 mV s^{-1}) while

after 300 s the growth rate decreases one order of magnitude. Neither scan rate nor temperature has a significant influence on passive film growth. The mass loss rate (dissolution) decreases exponentially with time.

- At the transpassive potential of 0.55 $V_{Ag/AgCl}$ the film grows from the beginning at constant rate of 0.49 nm min^{-1} at room temperature and 0.77 nm min^{-1} at 37°C. The observed constant mass loss rate indicates that the passive film at the transpassive potential is cracked or porous.
- The onset of the transpassive dissolution takes place at potentials above the transpassive potential as commonly defined by the increase in the current density on polarization curves. The latter corresponds well to the oxidation of Cr(III) oxide. This indicates that oxidation of Cr(III) to Cr(VI) is not sufficient to trigger the transpassive dissolution of CoCrMo.

Acknowledgments

We wish to express our gratitude to the Spanish Government, "Ministerio de Educación" for the economic support and the post-graduate grant (Ref.AP2007-01243) and "Ministerio de Ciencia e Innovación" for the financial support (Ref.MAT2011-22481), the assistance of N. Xanthopoulos with the XPS measurements and P. Mettraux with the PVD deposits and assistance with the scanning electron micrographs.

References

1. K. S. Katti, *Colloid. Surface. B*, **39**, 133 (2004).
2. Y. Okazaki, *Biomaterials*, **23**, 2071 (2002).
3. S. Virtanen, I. Milosev, E. Gomez-Barrena, R. Trebse, J. Salo, and Y. T. Konttinen, *Acta Biomater.*, **4**, 468 (2008).
4. I. Milosev and H.-H. Strehblow, *Electrochim. Acta*, **48**, 2767 (2003).
5. A. W. E. Hodgson, S. Kurz, S. Virtanen, V. Fervel, C.-O. A. Olsson, and S. Mischler, *Electrochim. Acta*, **49**, 2167 (2004).
6. A. Igual Muñoz and S. Mischler, *J. Electrochem. Soc.*, **154**, C562 (2007).
7. T. Hanawa, S. Hiromoto, and K. Asami, *Appl. Surf. Sci.*, **183**, 68 (2001).
8. T. Hanawa, *Mat. Sci. Eng. C-Mater. Biol. Appl.*, **24**, 745 (2004).
9. C. Fleury, A. Petit, F. Mwale, J. Antoniou, D. J. Zukor, M. Tabrizian, and O. L. Huk, *Biomaterials*, **27**, 3351 (2006).
10. M. A. Germain, A. Hatton, S. Williams, J. B. Matthews, M. H. Stone, J. Fisher, and E. Ingham, *Biomaterials*, **24**, 469 (2003).
11. A. Masse, M. Bosetti, C. Buratti, O. Visentin, D. Bergadano, and M. Cannas, *J. Biomed. Mater. Res.-A.*, **67B**, 750 (2003).
12. J. H. Dumbleton and M. T. Manley, *J. Arthroplasty*, **20**, 174 (2005).
13. I. Milosev and H. H. Strehblow, *J. Biomed. Mat. Res.*, **52**, 404 (2000).
14. S. Fukuzaki, H. Urano, and K. Nagata, *J. Ferment. Bioeng.*, **81**, 163 (1996).
15. M. Malmsten, *J. Colloid Interf. Sci.*, **207**, 186 (1998).
16. M. A. Khan, R. L. Williams, and D. F. Williams, *Biomaterials*, **17**, 2117 (1996).
17. S. Kanagaraja, I. Lundström, H. Nygren, and P. Tengvall, *Biomaterials*, **17**, 2225 (1996).
18. Y. Yan, A. Neville, and D. Dowson, *Tribol. Int.*, **40**, 1492 (2007).
19. N. J. Hallab, K. Mikecz, C. Vermes, A. Skipor, and J. J. Jacobs, *Mol. Cell. Biochem.*, **222**, 127 (2001).
20. A. Kocijan, I. Milosev, D. K. Merl, and B. Pihlar, *J. Appl. Electrochem.*, **34**, 517 (2004).
21. C. Valero Vidal and A. Igual Muñoz, *Corros. Sci.*, **50**, 1954 (2008).
22. C. Valero Vidal and A. Igual Muñoz, *Electrochim. Acta*, **54**, 1798 (2009).
23. C. Valero Vidal and A. Igual Muñoz, *Electrochim. Acta*, **55**, 8445 (2010).
24. E. Bettini, T. Eriksson, M. Boström, C. Leygraf, and J. Pan, *Electrochim. Acta*, **56**, 9413 (2011).
25. D. A. Buttry and M. D. Ward, *Chem. Rev.*, **92**, 1355 (1992).
26. V. Daujotis, D. Jasaitis, and R. Raudonis, *Electrochim. Acta*, **42**, 1337 (1997).
27. G. Sauerbrey, *Z. Phys.*, **155**, 206 (1959).
28. F. Galliano, C.-O. A. Olsson, and D. Landolt, *J. Electrochem. Soc.*, **150**, B504 (2003).
29. C.-O. A. Olsson and D. Landolt, *Electrochim. Acta*, **48**, 3999 (2003).
30. M. G. Verge, C.-O. A. Olsson, and D. Landolt, *Corros. Sci.*, **46**, 2583 (2004).
31. C.-O. A. Olsson, M. G. Verge, and D. Landolt, *J. Electrochem. Soc.*, **151**, B652 (2004).
32. P. Schmutz and D. Landolt, *Electrochim. Acta*, **45**, 899 (1999).
33. P. Schmutz and D. Landolt, *Corros. Sci.*, **41**, 2143 (1999).
34. D. Hamm, K. Ogle, C.-O. A. Olsson, S. Weber, and D. Landolt, *Corros. Sci.*, **44**, 1443 (2002).
35. C.-O. A. Olsson and D. Landolt, *Electrochim. Acta*, **48**, 1093 (2003).
36. C.-O. A. Olsson and D. Landolt, *J. Electrochem. Soc.*, **148**, B438 (2001).
37. C.-O. A. Olsson, D. Hamm, and D. Landolt, *J. Electrochem. Soc.*, **147**, 2563 (2000).
38. V. Payet, S. Brunner, A. Galtayries, I. Frateur, and P. Marcus, *Surf. Interface Anal.*, **40**, 215 (2008).
39. M. Herranen and J.-O. Carlsson, *Corros. Sci.*, **43**, 265 (2001).
40. F. Höök, J. Vörös, M. Rodahl, R. Kurrat, P. Böni, J. J. Ramsden, M. Textor, N. D. Spencer, P. Tengvall, J. Gold, and B. Kasemo, *Colloid. Surface. B*, **24**, 155 (2002).
41. I. Frateur, J. Lecoeur, S. Zanna, C.-O. A. Olsson, D. Landolt, and P. Marcus, *Electrochim. Acta*, **52**, 7660 (2007).
42. A. Ithurbide, I. Frateur, A. Galtayries, and P. Marcus, *Electrochim. Acta*, **53**, 1336 (2007).
43. A. Igual Muñoz and S. Mischler, *Inter-laboratory study on electrochemical methods for the characterisation of CoCrMo biomedical alloys in simulated body fluids*, European Federation of Corrosion by Maney Publishing on behalf of The Institute of Materials, Minerals & Mining, UK (2011).
44. S. Bruckenstein and M. Shay, *Electrochim. Acta*, **30**, 1295 (1985).
45. P. Kern and D. Landolt, *J. Electrochem. Soc.*, **147**, 318 (2000).
46. J. J. Kelly, K. M. A. Rahman, C. J. Durning, and A. C. West, *J. Electrochem. Soc.*, **145**, 492 (1998).
47. C.-O. A. Olsson and D. Landolt, *Corros. Sci.*, **46**, 213 (2004).
48. B. Brox and I. Olefjord, in *Proceedings of Stainless Steel* 1984, p. 134, The Institute of Metals, London (1985).
49. L. Wegrelius and I. Olefjord, in *Proceedings of 12th International Corrosion Congress*, 5B, p3887, NACE, Houston, TX (1993).
50. A. Savitzky and M. J. E. Golay, *Anal. Chem.*, **36**, 1627 (1964).
51. A. Ouerd, C. Alemany-Dumont, B. Normand, and S. Szunerits, *Electrochim. Acta*, **53**, 4461 (2008).
52. S. Tanuma, C. J. Powell, and R. Penn, *Surf. Interface Anal.*, **21**, 165 (1994).
53. S. Tanuma, C. J. Powell, and R. Penn, *Surf. Interface Anal.*, **35**, 268 (2003).
54. A. Kocijan, I. Milosev, and B. Pihlar, *J. Mater. Sci.-Mater. M.*, **15**, 643 (2004).
55. D. Hamm, C.-O. A. Olsson, and D. Landolt, *Corros. Sci.*, **44**, 1009 (2002).
56. P. Schmuki, S. Virtanen, A. J. Davenport, and C. M. Vitus, *J. Electrochem. Soc.*, **143**, 3997 (1996).
57. C. Valero Vidal, A. Olmo Juan, and A. Igual Muñoz, *Colloid. Surface. B*, **80**, 1 (2010).